JCTC Journal of Chemical Theory and Computation

Article

pubs.acs.org/JCTC

Conformational Dynamics of the FMN-Binding Reductase Domain of Monooxygenase P450BM-3

Rajni Verma,[†,‡] Ulrich Schwaneberg,[‡] and Danilo Roccatano*[,†]

[†]School of Engineering and Science, Jacobs University Bremen, Campus Ring 1, 28759 Bremen, Germany

[‡]Department of Biotechnology, RWTH Aachen University, Worringer Weg 1, 52074 Aachen, Germany

Supporting Information

ABSTRACT: In the cytochrome P450BM-3, the flavin mononucleotide (FMN) binding domain is an intermediate electron donor between the flavin adenine dinucleotide (FAD) binding domain and the HEME domain. Experimental evidence has shown that different redox states of FMN cofactor were found to induce conformational changes in the FMN domain. Herein, molecular dynamics (MD) simulation is used to gain insight into the latter phenomenon at the atomistic level. We have studied the effect of FMN cofactor and its redox states (oxidized and reduced) on the structure and dynamics of the FMN domain. The results of our study show significant differences in the atomic fluctuation amplitude of the FMN domain in both holo- and apoprotein. The change in the protonation state of FMN cofactor mostly affects its binding in holo-protein. In particular, the loops involved in the binding of the isoalloxazine ring (Lβ4) and ribityl side chain (Lβ1) adopt different conformations in both reduced and oxidized states. In addition, the reduced FMN cofactor mainly induces a conformational change in Trp574 residue (Lβ4) that is essential for controlling electron transfer (ET) within P450BM-3 domains. The structure of the apoprotein in solution remains mostly unchanged with respect to the crystal structure of the holo-protein. However, FMN binding loops were more flexible in apoprotein that might favor the rebinding of FMN cofactor. In the holo-protein simulation, the largest conformational changes in FMN cofactor are caused by the ribityl side chain. The isoalloxazine ring of FMN cofactor remains almost planar (~177°) in the oxidized state and bends along the N5−N10 axis at an angle of ~160° in the reduced state. The collective modes of the isoalloxazine ring were identical in both protonation states of FMN cofactor except the first eigenvector. In the reduced state, the isoalloxazine ring attains the butterfly motion as a dominant collective motion in the first eigenvector due to the bending along the N5−N10 axis.

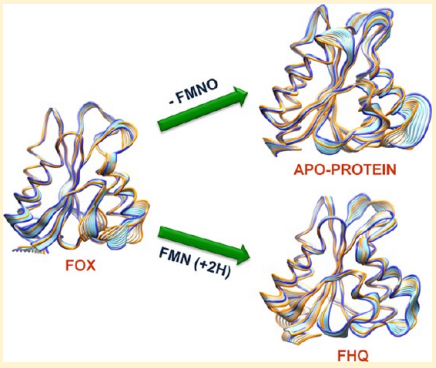

INTRODUCTION

Cytochrome P450 monooxygenases, the largest superfamily of heme-containing soluble proteins, spread widely in almost all domains of life, e.g., bacteria, yeast, insects, mammalian tissues, and plants.[1−3] They catalyze the oxidation of a wide variety of substrates involved in biosynthesis and biodegradation pathways, or in xenobiotic metabolism.[4] Cytochrome P450BM-3, isolated from *Bacillus megaterium*, is a multidomain, self-sufficient, NADPH-dependent flavoenzyme (class III bacterial P450).[5] As a pivotal member of its superfamily, it has been deeply studied as an important model system for the comprehension of structure/function relationships, and many structural and kinetic data are available in the literature.[6,7] The peculiar catalytic properties of this enzyme toward industrial applications have also been successfully enhanced by protein engineering.[8,9]

This enzyme is composed of two reductase domains (with FAD and FMN cofactors) and a P450 HEME domain (with a HEME cofactor) that are arranged on a single polypeptide chain as HEME−FMN−FAD from the N- to C-terminus. The transfer of two successive electrons from NADPH to a HEME cofactor is essential for the oxygenation reaction.[10−12] During the oxygenation reaction, the enzyme is reduced by NADPH, with electrons first transferred to the FAD cofactor of the FAD-binding domain then to the FMN cofactor of the FMN-binding domain and finally to the HEME iron in the substrate bound HEME domain. In this ET process, the FMN domain serves as a one- or two-electron mediator from the FAD cofactor to the HEME iron.[13] The FMN cofactor switches between a fully oxidized and a semiquinone state during catalytic turnover. The thermodynamically unstable anionic semiquinone state can reduce HEME iron. However, other P450s utilize FMN hydroquinone as the reduction species.[11−13] In the substrate free P450BM-3, the FMN cofactor stays in a thermodynamically stable hydroquinone state which is not able to reduce HEME iron.[11] The use of the anionic semiquinone state of the FMN cofactor as a reduction species makes P450BM-3 more efficient with a high turnover rate in comparison to other members of this family.[14] Therefore, the thermodynamic properties of the FMN moiety are mainly responsible for the unusual redox properties of P450BM-3. The protein environment has a strong influence on the latter mechanism by changing the redox potential of FMN and HEME cofactors.

Received: August 16, 2012
Published: December 10, 2012

The mutagenesis studies have shown that the conformation of FMN binding loops plays a critical role in stabilizing the different redox states of the FMN cofactor in the protein environment.[14,15] The insertion of a glycine residue in the *reface* (inner-FMN binding) loop is able to stabilize the neutral semiquinone state in P450BM-3 as observed in other diflavin reductases.[16]

Although experimental data of the isolated FMN domain in solution and the crystallographic structure[17,18] are available, a molecular dynamics (MD) study of this protein has not been reported. In this paper, the structural and dynamic properties of the FMN domain as a holo-protein, with the FMN cofactor in oxidized and reduced states and as an apoprotein, are investigated using classical MD simulations. The aim of this study is to understand the structural and dynamic properties of the protein in solution and the effect of the protonation state of the FMN cofactor on the conformational dynamics of the FMN cofactor and the whole protein. The paper is organized as follows. In the Methods section, the details of the simulations, in particular the refinement of the original GROMOS96 FMN parameters for the oxidized and reduced states of the FMN cofactors, are reported. In the Results section, the analysis of the simulation trajectories for the apo- and the holo-protein in the oxidized and reduced states is reported. The analysis will be focused on the structural and dynamic properties of the overall protein structure and of the FMN binding site as well as the FMN cofactor. Finally, in the Discussion and Conclusions, the results of the simulations will be discussed in the context of the experimental knowledge of the FMN domain, and a summary of the paper will be provided.

METHODS

Starting Coordinates. The starting coordinates of the FMN domain (residue 479−630) were taken from a non-stoichiometric complex of P450BM-3 (PDB ID: 1BVY, 2.03 nm resolution) which has one FMN domain with two HEME domains.[18] The crystallographic water (within a distance of 0.6 nm from the FMN domain) was also kept during system preparation for MD simulations.

Molecular Dynamics Simulation. Table 1 summarizes the systems used to perform MD simulations with the GROMOS96 43a1 force field.[19] The crystal structure[18] has the FMN cofactor in the oxidized state (FOX; see Figure 1a). The protonation of the FOX isoalloxazine ring at the N1 and N5 positions represents the reduced state of the FMN cofactor (FHQ) as indicated in Figure 1b. For the preparation of apoprotein simulation, the FMN cofactor was removed from the crystal structure of the FMN domain.

Table 1. Simulation Summary of the P450BM-3 FMN Domain in Water

FMN domain[a]	no. of atoms	no. of solvent molecules	no. of counterions	simulation length (ns)
oxidized (FOX)	33483	10650	14	50
reduced (FHQ)	33491	10652	14	50
apo protein (APO)	33482	10662	13	50

[a]The abbreviations FOX, FHQ, and APO are used in the rest of the manuscript for the FMN domain in oxidized, reduced, and apoprotein, respectively.

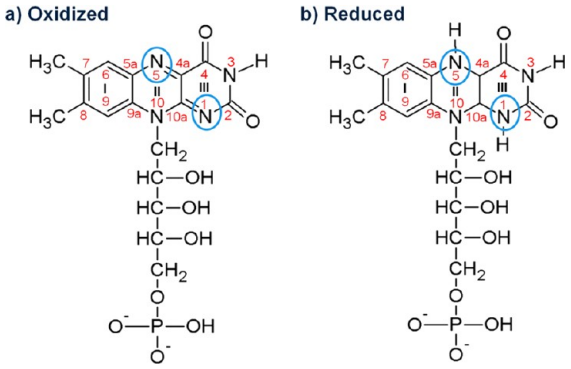

Figure 1. The schematic representation of the FMN cofactor in oxidized (a) and reduced (b) states with atomic numbering of the isoalloxazine ring.[20] N1 and N5 atoms, in blue ovals, highlight the protonation positions. ChemSketch[21] was used to draw the figures.

In all simulations, the FMN domain was centered in a cubic box. The sizes of the simulation boxes were set to have at least a minimal distance between the solute and any side of the box larger than 0.80 nm. The FMN domain was then solvated by stacking equilibrated boxes of solvent molecules to fill completely the simulation box. All solvent molecules with any atom within 0.15 nm from the atoms of protein were removed. The SPC water model[22] for the water molecule was used. The GROMOS96 force field[19] was used for the FMN cofactor. Additional improper dihedrals were introduced to adopt the conformation of the isoalloxazine ring as observed in the crystallographic structure and molecular geometry optimization of flavin in both redox states, reported in Table S1 (for FOX) and Table S2 (for FHQ) of the Supporting Information (SI).[23,24]

In the isoalloxazine ring of the FMN cofactor, the bending angle (δ) and puckering angle (ρ) were calculated along the N5−N10 axis using v_1, v_2, a_1, a_2, and c vectors, as shown in Figure 2. In FOX, the isoalloxazine ring was kept close to planar, while the bending angle of ∼160° was used for FHQ. Sodium counterions were added by replacing solvent molecules at the most negative electrostatic potential to provide a total charge of the box equal to zero. The protonation state of residues in the protein was assumed to be the same as that of the isolated amino acids in solution at pH 7. The LINCS[25] algorithm was used to constrain all bond lengths, and the SETTLE[26] algorithm was used for solvent molecules. Electrostatic interactions were calculated by using the particle mesh Ewald method.[27] For the calculation of the long-range interactions, a grid spacing of 0.12 nm combined with a

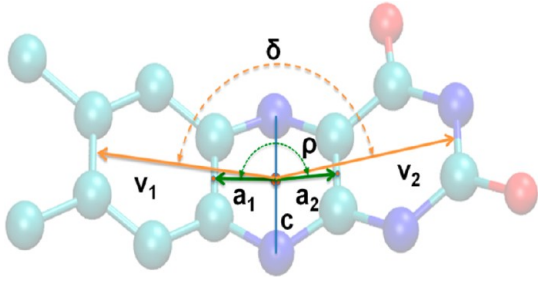

Figure 2. The schematic structure of the isoalloxazine ring to define the bending angle (δ) and puckering angle (ρ) using the vectors v_1, v_2, a_1, a_2, and c.

dx.doi.org/10.1021/ct300723x | J. Chem. Theory Comput. 2013, 9, 96−105

Table 2. Summarizing MSA of the FMN Domain of P450BM-3 and Its Homologous Structures and the Characterization of Their FMN-Binding Pocket

					FMN binding pocket			
PDB ID	organism	protein[a]	RMSD (nm)	max. sequence identity (%)	volume	hydrophobicity	solvent accessibility	polarity
1BVY	*Bacillus megaterium*	CPR	0.000	100.00	601.82	358.17	16.69	11
1B1C	*Homo sapiens*	CPR	0.134	30.26	508.28	299.54	25.26	11
1JA1	*Rattus norvegicus*	CPR	0.135	30.26	594.28	313.50	24.65	12
2BF4	*Saccharomyces cerevisiae*	CPR	0.135	25.00	554.08	354.37	11.29	12
1YKG	*Escherichia coli*	SiR-FP	0.172	19.86	639.03	354.39	20.88	15
3HR4	*Homo sapiens*	NOS	0.144	23.68	466.78	258.09	14.44	12
1F4P	*Desulfovibrio vulgaris*	Fld	0.214	23.13	558.02	340.19	10.82	15

[a]CPR: cytochrome P450 reductase. SiR-FP: sulfite reductase. NOS: nitric oxide synthase. Fld: flavodoxin.

fourth-order B-spline interpolation were used to compute the potential and forces between grid points. A nonbonded pair-list cutoff of 1.4 nm was used and updated every five time steps. Simulated systems were first energy minimized, using the steepest descent algorithm, for at least 2000 steps in order to remove clashes between atoms that were too close. After energy minimization, all atoms were given an initial velocity obtained from a Maxwell−Boltzmann velocity distribution at 300 K to start MD simulations. All systems were initially equilibrated using100 ps of a MD run with position restraints on the heavy atoms of the solute to allow relaxation of the solvent molecules. Berendsen's thermostat[28] was used to keep the temperature at 300 K by weak-coupling the systems to an external thermal bath with a relaxation time constant τ = 0.1 ps. The pressure of the system was kept at 1 bar using the Berendsen's barostat[28] with a time constant of 1 ps. After the equilibration procedure, position restraints were removed, and the system was gradually heated from 50 to 300 K over 200 ps of simulation. Finally, a production run was performed at 300 K for 50 ns for all systems. All simulations and analyses of trajectories were performed using the GROMACS (version 4.07) software package.[29] The crystal structure of the FMN domain was used as the reference structure for the analysis in all simulations.

Cluster Analysis. A cluster analysis was performed to characterize the conformational diversity of the structures generated during the MD simulations. The cluster analysis was performed using the Gromos clustering algorithm.[30] In this method, a cutoff criterion on the root-mean square deviation (RMSD) cutoff, based on the root-mean square differences of selected atom among the conformations obtained from the simulations, is used to assign a structure in a cluster. A RMSD cutoff of 0.10 nm was used to determine neighboring backbone atom conformations of the FMN domain. The conformation with the least deviation from other members of the cluster is used as the representative structure of the clusters. For the cluster analysis of the FMN cofactor in the protein environment, the RMSD cutoff was reduced to 0.04 nm to discriminate among the less varying conformations. A total of 10 000 structures were sampled every 5 ps in the 50 ns of simulations for the analysis.

FMN Binding Site Analysis. The FMN binding site of the holo-protein and apoprotein were tracked throughout the MD simulation using the MDpocket method.[31] The analysis was performed on a total of 5000 snapshots after taking every 50th frame from the trajectories. The pocket volume analysis was performed on aligned MD snapshots with a minimum alpha sphere size of 3 Å; the minimum number of alpha spheres close to each other for the alpha sphere clustering equal to the number of iterations to perform the pocket volume calculation using the Monte Carlo algorithm was set to 5000. The grid file generated by the first MDpocket run (iso-value = 0.7) was used to extract the grid points for the FMN binding pocket. The grid file of the FMN binding pocket was edited manually by deleting some grid points using PyMOL[32] for better representation of the FMN binding site in the FMN domain. The FMN binding grid file was used with the aligned snapshots to track the changes in the FMN binding site during the simulation.

Multiple Structural Alignment of the FMN Domain. The homologous structures of the FMN domain were obtained by performing BlastP[33] against the PDB database.[34] The protein sequences with an identity greater than 20% were taken into account for further analysis. Six structures were selected as homologous to the FMN domain of P450BM-3 after manually removing the redundant entries from the BlastP results (summarized in Table 2). Multiple structural alignment (MSA) was performed on selected structures taking the FMN domain as a reference structure with a maximum RMSD cutoff of 0.5 nm using a UCSB chimera.[35]

Principal Component Analysis. A principal component analysis was performed to assess the conformational space in the biomolecules during simulation. Details of the methods can be found elsewhere.[36,37] The backbone atoms (C_α, C, and N, total 4614 atoms) of the FMN domain were used to explore the conformational subspace in the holo- and apoprotein. For the FMN cofactor, the heavy atoms of the isoalloxazine ring (18 atoms) were used for PCA. The displacements along different eigenvectors were calculated by projecting the atomic coordinates on eigenvectors and superimposing them using the UCSF Chimera visualization tool.[35] The comparison of eigenvectors obtained from different simulations was performed using the root-mean-square inner product (RMSIP),[38] which is defined in eq 1.

$$\mathrm{RMSIP} = \sqrt{\frac{1}{N}\sum_{i=1}^{m}\sum_{j=1}^{m}(\mathbf{v}_i\cdot\mathbf{u}_j)^2} \quad (1)$$

where v_i and u_j are the ith and jth eigenvectors of two different m dimension subspaces of the two systems. RMSIP gives a simple measure to assess the dynamical similarity of eigenvectors.[38] The convergence of the selected modes was performed by comparing the RMSIPs calculated from the MD trajectories of 50 ns.

RESULTS

FMN Domain: Structural and Dynamical Properties. Figure 3 shows the backbone root-mean-square deviation (RMSD) of the FMN domain as the apo- and holo-protein

dx.doi.org/10.1021/ct300723x | J. Chem. Theory Comput. 2013, 9, 96−105

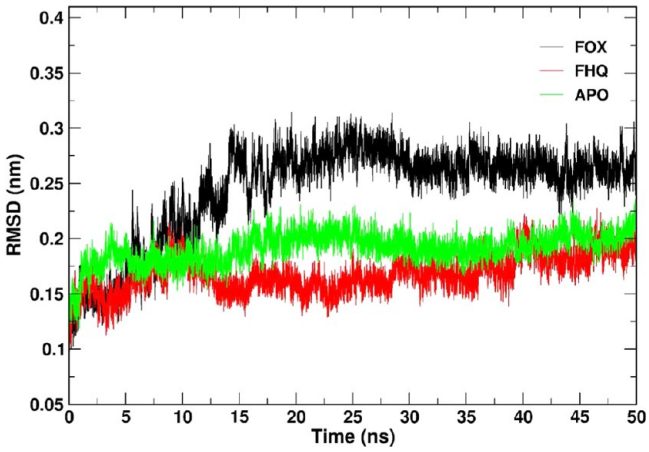

Figure 3. Backbone RMSD with respect to the crystal structure as a function of time for APO (in green) and the holo-protein in FOX (in black) and FHQ (in red).

with the FMN cofactor in the oxidized and reduced states. In FOX, the RMSD curve stabilizes to a plateau with an average value of 0.24 ± 0.04 nm after a rapid increase in the first 15 ns of simulation. In the first 10 ns of simulation, FHQ follows the same trend as observed in FOX. However, after 15 ns, the RMSD of FHQ stabilizes to an average value of 0.16 ± 0.01 nm lower than the one in FOX. In APO, the FMN domain remains stable throughout the simulation with an average RMSD value of 0.19 ± 0.01 nm after the short equilibration of ~5 ns. For all of the simulations, the average radius of gyration (Rg) did not show appreciable variations from the crystal structure value (1.45 nm).

The FMN domain has a highly classical flavodoxin fold with five parallel β-sheets (β1−β5) that are surrounded by four α-helices (α1−α4). The loop regions together with irregular structures (coils and turns) are named according to the secondary structure element, α(-helix) or β(-sheet), preceding them. The FMN cofactor is surrounded by three loops that succeed β sheets and are hence named Lβ1, Lβ3, and Lβ4 for the ribityl binding loop (residues 488−491) and inner (*re face* residues 534−544), and outer (*si face* residuse 571−579) FMN binding loop, respectively. The crystallographic protein secondary structure, calculated using the DSSP method,[39] was preserved during the simulation of FOX, FHQ, and even in the APO simulations (see Figure S1 of SI).

In Figure 4a and b, the backbone RMSD and RMSF per residue with respect to the crystal structure are reported, respectively. The FMN domain with labeled helices and loops is reported in Figure 4c. Residues with large RMSD and RMSF values correspond to loop regions (represented by gray colored bars in Figure 4a and b) and to the N- and C-termini. In all simulations, the largest deviations and fluctuations were observed in the Lβ3 and Lβ4 FMN binding loops (black horizontal bars in Figure 4a and b) and Lβ2 and Lα2 loops, which are present opposite to the FMN binding site. The Lα2 loop shows the highest deviation in FOX. In APO, the deviations and fluctuations are mainly observed in the FMN binding loops (especially in the Lβ1 loop) that also occupy the FMN binding cavity during simulation.

Cluster Analysis of FMN Domain. The total numbers of clusters observed in FOX, FHQ, and APO are 11, 12, and 7, respectively. The first two clusters account for 80.26% and 79.25% of the population for FOX and FHQ, respectively. The first cluster contributes 47.10% in FOX and 60.07% in FHQ. The second cluster represents 33.16% and 19.18% of the total population in FOX and FHQ, respectively. In APO, even the first cluster covers 85.17% of the population. The apoprotein shows the least conformational diversity during the simulation. However, the difference in the population of clusters in the holo-protein indicates that the FMN protonation state notably influences the conformation of the FMN domain.

In Figure 5a, b, and c, the representative conformations of the first two clusters of FOX and FHQ and the first cluster of APO are superimposed with the crystal structure (in sky blue) and shown in cartoon representation. Major differences occur in loop regions as well as in N- and C-termini. In particular, slightly larger deviations are present in FMN binding loops in FOX and FHQ. On the contrary, the FMN binding region in

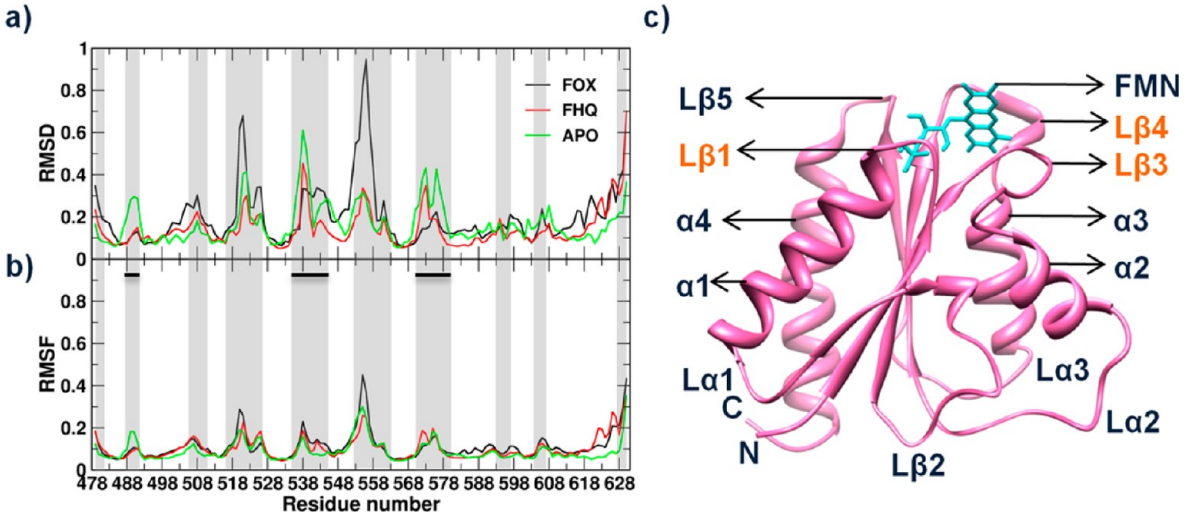

Figure 4. Backbone RMSD (a) and RMSF (b) per residue with respect to the crystal structure for FOX (black), FHQ (red), and APO (green). Vertical bars in gray color show the loop regions. Loops surrounding the FMN cofactor are shown in black horizontal bars. (c) The FMN domain in pink and FMN cofactor in cyan color with labeled helices and loop regions. The FMN binding loops are labeled in orange color. N and C represent the amino and carboxy termini of the FMN domain.

dx.doi.org/10.1021/ct300723x | J. Chem. Theory Comput. 2013, 9, 96−105

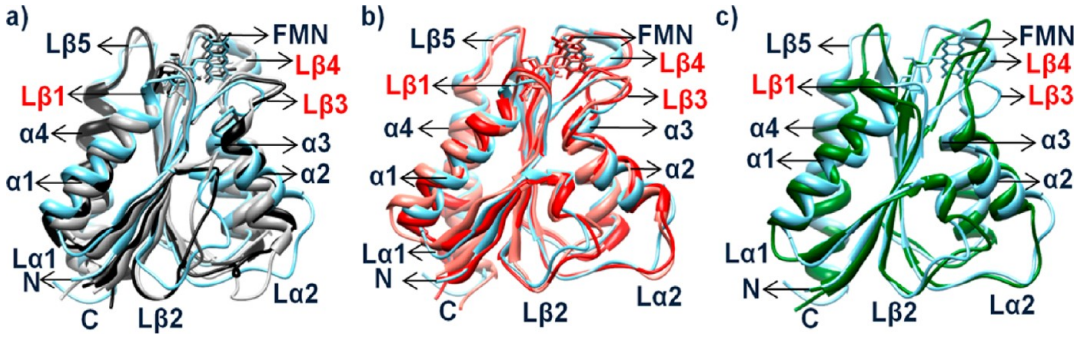

Figure 5. The conformation of first two clusters of (a) oxidized (black and gray), (b) reduced (red and coral), and (c) apoprotein (green) superimposed with the crystal structure (in sky blue). Loops and helices (α1, α2, α3, and α4) are labeled. FMN binding loops are labeled in a red color. The labeling of loops belongs to the secondary structure succeeding them.

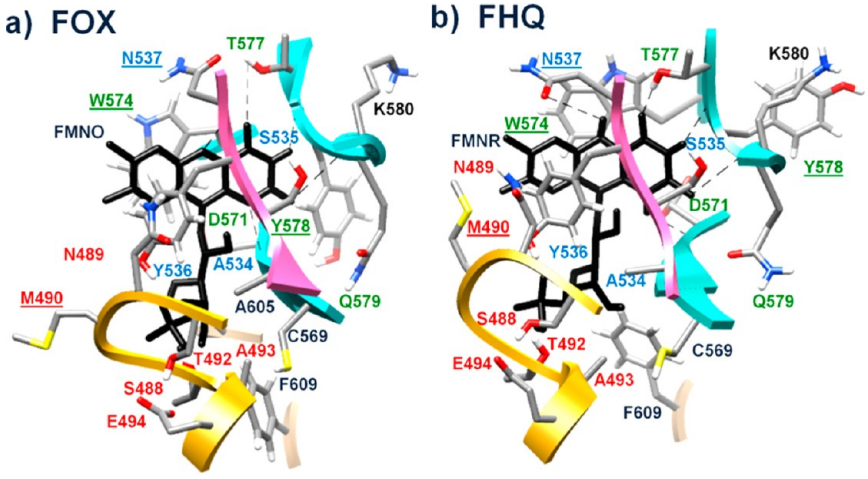

Figure 6. (a,b) The FMN binding site from the representative structures of the first cluster for FOX and FHQ, respectively. The represented residues are within 0.4 nm from the FMN cofactor (in black). FMN binding loops Lβ1, Lβ3, and Lβ4 are shown as the ribbon of yellow, pink, and cyan, respectively. The residues are labeled in red, blue, and green as part of Lβ1, Lβ3, and Lβ4, respectively. Dashed lines show hydrogen bonds between isoalloxazine and surrounding residues. The underlined labels indicate the residues that have a major change in conformation after the change in the redox state of the FMN cofactor.

APO is the most deviating part of the FMN domain. The loop regions Lβ2 and Lα2 are also affected by the presence and the protonation state of the FMN cofactor. In FOX, Lβ2 and Lα2 show larger deviations than in FHQ and APO, as evidenced by the conformation of the first two clusters (see Figure 5). The Lα2 loop flips inward with higher deviation from the crystal structure in the first two clusters of FOX.

FMN Binding Site. Figure 6 represents the FMN binding site in detail using the representative structure of the first cluster of FOX (Figure 6a) and FHQ (Figure 6b). The hydrogen bonds between the FMN domain and cofactor were calculated for a distance between the acceptor and hydrogen donor of $\leq$0.35 nm and an angle among acceptor, donor, and acceptor of $\leq$30°.

The occurrence of hydrogen bonds that are observed in the crystal structure between the FMN domain and the isoalloxazine ring of the FMN cofactor are reported in Figure S2 in the SI for the simulation of FOX (in blue) and FHQ (in red). NMR spectroscopy studies of the protein in solution have also evidenced the hydrogen-bonding network involving N1, C2O, N3, C4O, and N5 atoms of the isoalloxazine ring.[14,40] In the crystal structure, the hydrogen atom from the backbone amino group (NH) of Asn537 was involved in a hydrogen bond formation with the N5 atom of the isoalloxazine ring (NH−N5) with a distance of 0.175 nm. The same hydrogen bond was observed in the first 15 ns of FHQ simulation (in Figure S2a). However, with the N5 atom in FHQ being a hydrogen donor due to the protonation, a hydrogen bond with the oxygen from the side chain carboxamide group ($-CONH_2$) of Asn537 ($-(NH_2)CO-HN5$) was observed in the last 25 ns of simulation.

In the crystal structure and simulations, the stable hydrogen bonds were observed at oxygen (O2) and nitrogen (N3H) of the isoalloxazine ring with the hydrogen of the backbone amino group of Gln579 (NH−O2) and the oxygen from the backbone carbonyl group (CO) of Thr577 (N3H−OC), respectively. The O4 position was involved in hydrogen bond formation with hydrogen of the hydroxyl group of Thr577 (OH−O4) in the first 15 ns of simulation of FOX, but it occurred throughout the whole FHQ simulation. Atom N1 was observed to form a hydrogen bond with a backbone amino group of Asp571 (NH−N1) in the crystal structure and FOX. However, in the FHQ simulation, the occurrence of this bond (NH−N1H) was very low.

The change in protonation state of the FMN cofactor affects its binding in the FMN domain. FHQ strengthens the hydrogen-bonding network between the ribityl side chain and phosphate moiety of the FMN cofactor and domain. In FHQ, the phosphate group of the FMN cofactor forms stronger hydrogen bonds with the residues of the Lβ1 loop than in FOX

dx.doi.org/10.1021/ct300723x | J. Chem. Theory Comput. 2013, 9, 96−105

(shown in Figure S2b). The first hydroxyl group of the ribityl side chain was involved in strong hydrogen bonding with the carbonyl oxygen of Ser537 (OH−OC) in FOX and FHQ. The third hydroxyl group of the ribityl side chain shows a stronger hydrogen bond with the Thr492 hydroxyl in FOX than in FHQ. The latter was also observed to form a hydrogen bond with the carbonyl oxygen of Cys569 in FHQ.

In FHQ, the tighter binding of the FMN cofactor with a stronger hydrogen-bonding network between flavin and protein than in FOX induces the conformational change in FMN binding loops Lβ1, Lβ3, and Lβ4. The major conformational change was observed in the orientation of the Trp574 residue due to the protonated N5 position in the isoalloxazine ring in FHQ (Figure 6b). The indole ring of Trp574 was nearly coplanar to the isoalloxazine ring of the FMN cofactor in the crystal structure.[17] Experimentally, the Trp574 conformation was observed to be critical to the FMN binding and found to be involved in ET tunneling from FMN to HEME. In FOX, the indole ring of Trp574 remains in the same conformation as in the crystal. In FHQ, it rotates to another configuration not aligned to the isoalloxazine ring. This rotation is a consequence of the steric hindrance induced by the conformation change in the reduced isoalloxazine ring.

The change in the volume, hydrophobicity, solvent accessibility, and polarity of the FMN binding site are reported in Figures S3a,b,c,d, respectively in the SI during the simulation of FOX (in black), FHQ (in red), and APO (in green). In APO, the absence of the FMN cofactor promotes a rearrangement of the FMN binding site. After rearrangement, the side chains of amino acids of FMN binding loops replaced the initial water molecules and occupied the cavity after ∼5 ns of simulation. FOX shows larger variation in the geometric properties of the FMN binding pocket than FHQ. Major changes were observed in the volume of the FMN binding pocket after the change in protonation state of the FMN cofactor with averages 429 ± 86 and 357 ± 45 for FOX and FHQ, respectively. In FHQ, the pocket volume showed less variation than in FOX (see Figure S3a). The hydrophobicity (Figure S3b) and polarity (Figure S3d) of the FMN pocket are slightly perturbed in the first 15 ns of simulation and then converge to the same values in both FHQ and FOX simulations.

Comparison of the FMN Domain of P450BM-3 with Homologous Structures. In Table 2, the summary of MSA for the FMN domain of P450BM-3 and its homologous structures (in the SI, see Figure S4 for MSA and Figure S5 for conservation patterns mapped on FMN domain of P450BM-3) is reported. The ribityl side-chain binding region is the most conserved region in the FMN domain since it is responsible for the tight binding of the FMN cofactor. Among the cytochrome P450 reductases (CPR), the P450BM-3 one has the higher volume of FMN binding site with a higher hydrophobicity and lower polarity. The solvent accessibility of the FMN binding pocket was found to be in the middle of other homologous proteins. Together, all of these differences in the properties of the FMN-binding pocket of P450BM-3 result in a better catalytic turnover than in other P450 monooxygenases.[14,17]

Principal Component Analysis of the FMN Domain. The cumulative relative positional fluctuation (RPF) of the first 20 eigenvectors accounts for 82%, 79%, and 75% of the total RPF in the simulation of FOX, FHQ, and APO, respectively. The convergence of the trajectory has been analyzed by comparing the RMSIP value for the first 20 eigenvectors obtained from the PCA of MD trajectories (50 ns). The RMSIP values calculated by the two halves of the trajectories resulted in 0.563, 0.624, and 0.594 for the simulation of FOX, FHQ, and APO, respectively. The relatively high values of the RMSIP for the trajectories indicate a good convergence of the essential eigenvectors. The first two eigenvectors cover the 50%, 41%, and 32% (with 32% and 29% and 20% contribution just from the first eigenvector) of the total fluctuations in FOX, FHQ, and APO, respectively. The inner product (IP) values for the first two eigenvectors obtained from the inner product matrix of two trajectories are reported in Table 3. The inner product of the first eigenvector in all simulations was found to be less than 0.350, which shows that the most important essential mode is different for the three systems.

Table 3. RMSIP Values of the First Two Eigenvectors Obtained from the 50 ns Trajectories of FOX, FHQ, and APO

		inner product	
		first eigenvector	second eigenvector
FOX/FHQ	first eigenvector	0.143	0.400
	second eigenvector	0.485	0.414
FOX/APO	first eigenvector	0.268	0.156
	second eigenvector	0.033	0.156
FHQ/APO	first eigenvector	0.351	0.281
	second eigenvector	0.183	0.169

Figure 7a represents the RMSF of the backbone atoms in the first and second eigenvectors of FOX (black), FHQ (red), and APO (green). The corresponding tridimensional representations obtained after the projection of first and second eigenvectors on MD trajectories are reported in Figure 7b, c, and d for FOX, FHQ, and APO, respectively. In all simulations, the residues of C terminal and long loop regions, Lβ2 and Lα2, that are present opposite the FMN binding site show higher fluctuations and together constitute the collective motions in the first eigenvector. In the first eigenvector of FOX, the collective motion is restricted to Lβ2, Lβ3, and Lα2 loops and the C terminal region and have higher fluctuations. In the second eigenvector of FOX, a higher fluctuation was shown by C terminal residues and Lα1, Lβ2, and Lα2 loops. FHQ shows higher fluctuations in Lα1, Lα2, and Lβ4 loops and C and N termini in the first eigenvector. The second eigenvector of FHQ shows higher fluctuations in Lα2, Lβ2, and Lβ4 loops. The first eigenvector of APO shows higher fluctuations in Lβ1, Lβ2, and Lα2 loops and the C terminal, while the second eigenvector shows them in the Lα2 loop and in all of the FMN binding loops. The higher fluctuations constituting the collective motion in the first eigenvector were observed in the inner FMN binding loop Lβ3 for FOX, outer FMN binding loop Lβ4 for FHQ, and ribityl side chain binding loop Lβ1 for APO.

Figure 8 shows the crystallographic structure complex of HEME with the FMN domain with labeled helices, cofactors, and FMN binding loops. In the crystal structure, the α1 helix is involved in direct or water mediated contacts with the HEME domain, and the outer FMN binding loop (Lβ4) interacts with the peptide preceding the HEME binding loop (K/L loop).[18] These interaction sites are crucial for the ET from FMN to HEME. Higher fluctuations observed in Lβ4 and α1 helix regions in the first eigenvector of FHQ might be related to the inhibition of electron transfer from FMN to HEME by a

dx.doi.org/10.1021/ct300723x | J. Chem. Theory Comput. 2013, 9, 96−105

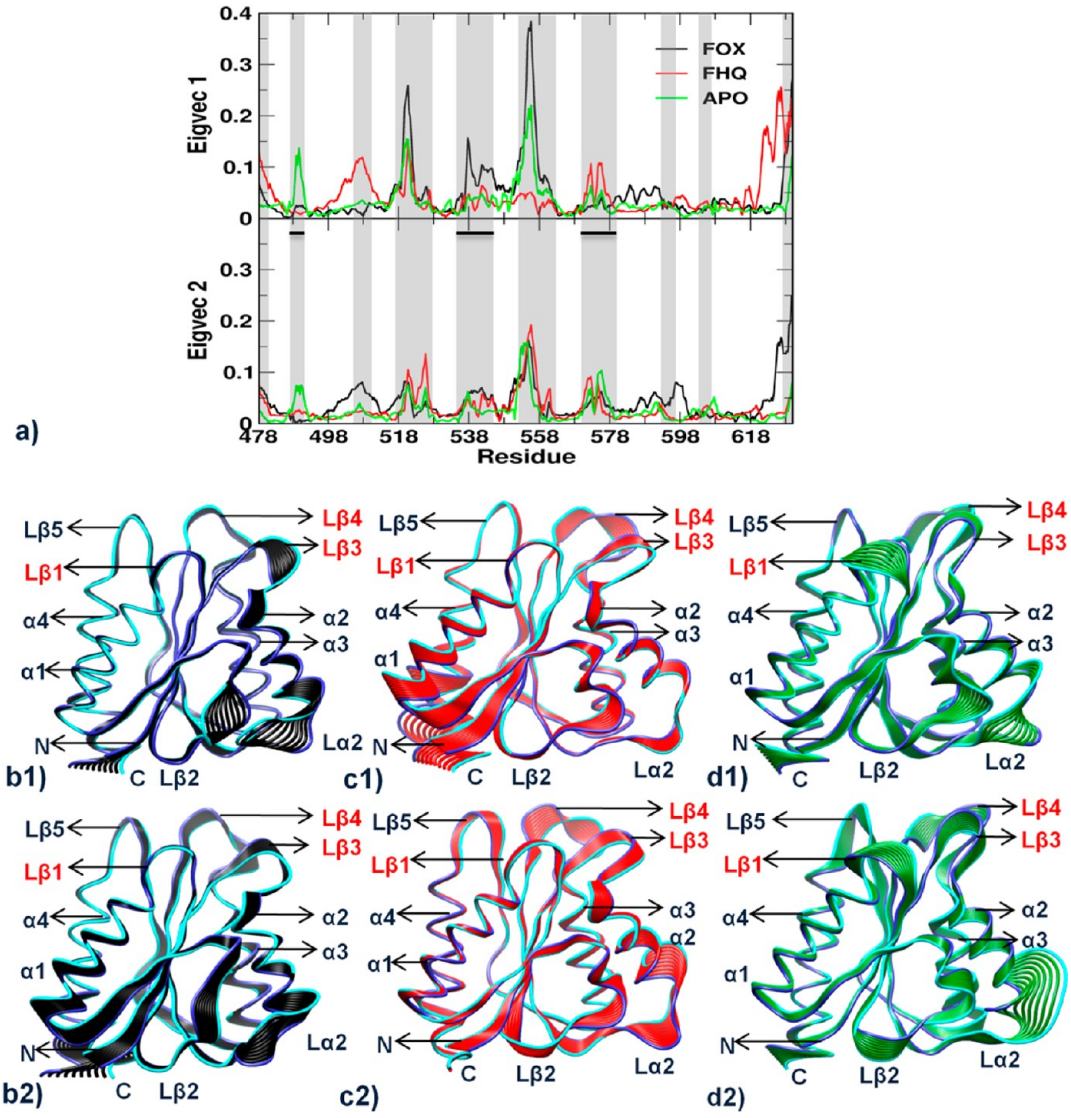

Figure 7. (a) RPF associated with eigenvectors. Vertical bars in a gray color show the loop regions. FMN binding loops are shown as black horizontal bars. (b) Representation of the RMSF of the protein backbone atoms along first and second eigenvectors after projection of the trajectory of FOX (black), FHQ (red), and APO (green) on the corresponding eigenvectors. The 10 sequential frames representing the extension of the fluctuations in FOX (b), FHQ (c), and APO (d) trajectories along the first and second eigenvectors are reported. The first extreme is shown in blue color and the last extreme in cyan. Loops and helices are labeled. Labels in red show the FMN binding loops. N and C indicate the N- and C-termini of the protein.

reduced state of the FMN cofactor as observed experimentally.[11] In the first eigenvector of FOX, the higher fluctuation was restricted to the residues of the inner FMN binding loop Lβ3 and loops, opposite to the FMN binding site, Lα2 and Lβ2. So the latter defined region is found opposite to the region of probable HEME binding surface in the crystal structure, so the collective motion constituted by this region in FOX might be related to the electron transfer from FAD to FMN, and it could be the probable binding site for the FAD domain. In APO, the local structure remains conserved with highly flexible FMN binding loops that help to rebind the FMN cofactor in apoprotein and working again as a holo-protein, as found experimentally.[41]

FMN Cofactor: Structural and Dynamical Properties. The conformational changes of the FMN cofactor induced by the surrounding protein environment were studied for both redox states. The RMSD and RMSF of the phosphate group atoms for both states show higher fluctuations and deviations than other heavy atoms of the FMN cofactor (see Figure S6a and b of the SI). Furthermore, the phosphate group of the FMN cofactor in the oxidized state deviates more from the crystal structure and with higher fluctuations than it does in the reduced state. This is consistent with the observed variations of the hydrogen-bonding network between the FMN cofactor and the protein.

Figure 9a shows the distribution of the value of δ angles of the isoalloxazine ring (see Figure 2) in FOX and FHQ. For the oxidized state of the FMN cofactor, the values are normally distributed in the range from 170° to 180° with the peak centered at 177°. In the reduced state, the distribution of δ has a larger width. The reduced state of FMN shows a distribution ranging from 154° to 171° with a peak at 162°. For the latter case, the average value is consistent with quantum mechanical calculations in a vacuum of the isoalloxazine ring in the reduced state[24,42] that give a value for δ = ~160°.

dx.doi.org/10.1021/ct300723x | J. Chem. Theory Comput. 2013, 9, 96−105

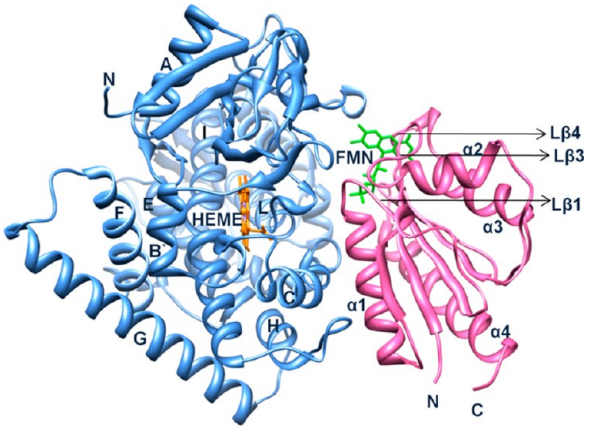

Figure 8. FMN domain (in pink) complex with the P450 HEME domain (in blue) in crystal structure (1BVY[18]). The HEME cofactor is represented in orange and the FMN cofactor, in green. Helices and N- and C-termini are labeled in both domains. Labels Lβ1, Lβ3, and Lβ4 show the FMN cofactor binding loops in the FMN domain.

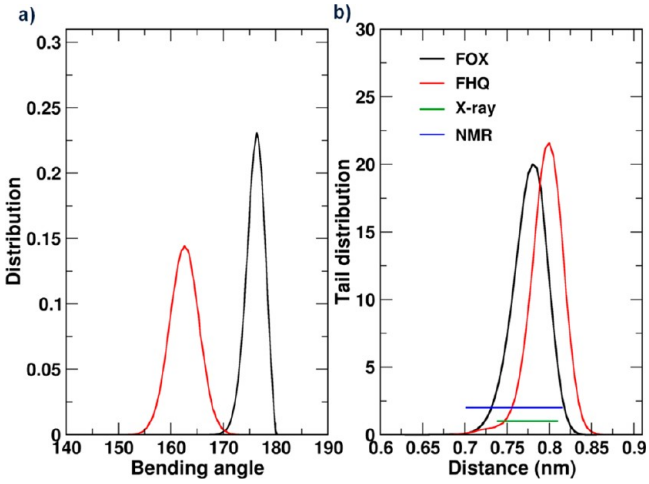

Figure 9. Distribution of (a) angles calculated at the N5−N10 axis of the isoalloxazine ring along the 50 ns simulation of FOX (in black color) and FHQ (in red color) with a 0.3 bin width and (b) the beginning to end distance of the ribityl side chain along a 50 ns simulation for FOX and FHQ (0.007 bin width) and in X-ray (in green color) and NMR (in blue color) homologous structures of the FMN domain.

Figure 9b shows the distribution of the beginning to end distance for the ribityl side chain of the FMN cofactor in FOX, FHQ, and the homologous structures of the FMN domain with the FMN cofactor in the oxidized state. For the crystallographic and NMR homologous structures, the distances range from 0.73 to 0.8 nm and 0.70 to 0.82 nm, respectively. The distance observed in the crystal structure of the FMN domain was 0.77 nm. The distances obtained from the FOX and FHQ simulations are distributed in the range of 0.61 to 0.90 nm with the main peaks at 0.78 and 0.80 nm, respectively. The beginning to end distance for the ribityl side chain in the simulations and in NMR and crystallographic studies was consistent and distributed in the same range.

Cluster Analysis of FMN Cofactors. The cluster analysis was performed on the heavy atoms of the FMN cofactor using the crystal structure as a reference and a cutoff of 0.04 nm in the protein environment. The first cluster comprises 87% and 99% of the total 13 and 8 clusters in FOX and FHQ, respectively.

The cumulative sum of the number of clusters obtained from different simulations as a function of time is reported in Figure S7 of the SI. Both the simulations reached a plateau, which indicates a sufficient sampling of conformational space along the trajectories. The representative structures of the first cluster of FOX (in black) and FHQ (in red) are reported in Figure S7 in the SI. The conformational flexibility of the ribityl side chain was observed to be mainly responsible for the conformational diversity of clusters in both the simulations. The reduced number of clusters in the FHQ simulation is consistent with the small RMSF fluctuations of the ribityl side chain. The preferred conformation for the FMN cofactor in both redox states is characterized by a partially elongated ribityl side chain (see Figure S7 in the SI).

Principal Component Analysis of FMN Cofactors. The first eight eigenvectors cover ∼79% of the total RPF in both the simulations. In the protein environment, RPF covers ∼25% and ∼27% by the first eigenvector in FOX and FHQ, respectively. The superimposition of the first and last extreme structures of the isoalloxazine ring generated by the projection of the first eight eigenvectors on the trajectory of FOX is shown in Figure 10. In the first eigenvector, a symmetric bending mode of the ring is present in both of the simulations. However, the reduced state (Figure 10, 1b) manifests a "butterfly wing" bending mode around the N5−N10 axis. This type of vibrational mode has been also reported in previous experimental and quantum mechanics studies.[23,24,42] The other seven modes show similar eigenvectors in both states. The second most dominant motion is the twisting of the isoalloxazine ring along the main isoalloxazine axis. The observed collective modes are in qualitative agreement with the vibrational normal modes obtained from resonance Raman spectroscopy measurements and QM calculations for the Lumiflavin.[20,42] In addition, surface enhanced resonance Raman scattering studies of the free FMN cofactor and in the FMN domain indicate evidence of the presence of vibrational modes resulting from atomic displacement of atoms like C4, O, C4a, C10a, C5a, and C9a.[43] These experimental observations are consistent with higher fluctuations in correspondence with these atoms observed in PC modes from the first eight eigenvectors of our simulations.

■ DISCUSSION AND CONCLUSIONS

MD simulations have been performed on the FMN binding reductase domain of monooxygenase P450BM-3 using the FMN cofactor in oxidized and reduced states to understand the effect of the change in protonation state of the isoalloxazine ring on the conformation and dynamics of the FMN domain and cofactor. The results of the simulations showed that the change of the protonation state in the reduced FMN affects the overall structure and dynamics of the FMN domain in solution. In particular, the structural and dynamic properties of the *si*-face FMN binding loop (Lβ3) are strongly influenced by the change in protonation of the FMN cofactor (in FOX). In the apoprotein, the overall local structure of the protein remains preserved, but higher fluctuations were observed in the FMN binding loops. The latter effect can explain the experimental finding of reversible rebinding of the FMN cofactor in apoprotein.[40,44,45] The loop Lβ2 was observed to contribute mainly on the collective modes of the FMN domain as holoprotein or apoprotein, which is also in agreement with the solution structure of the flavodoxin-like domain of *E. coli*

dx.doi.org/10.1021/ct300723x | J. Chem. Theory Comput. 2013, 9, 96−105

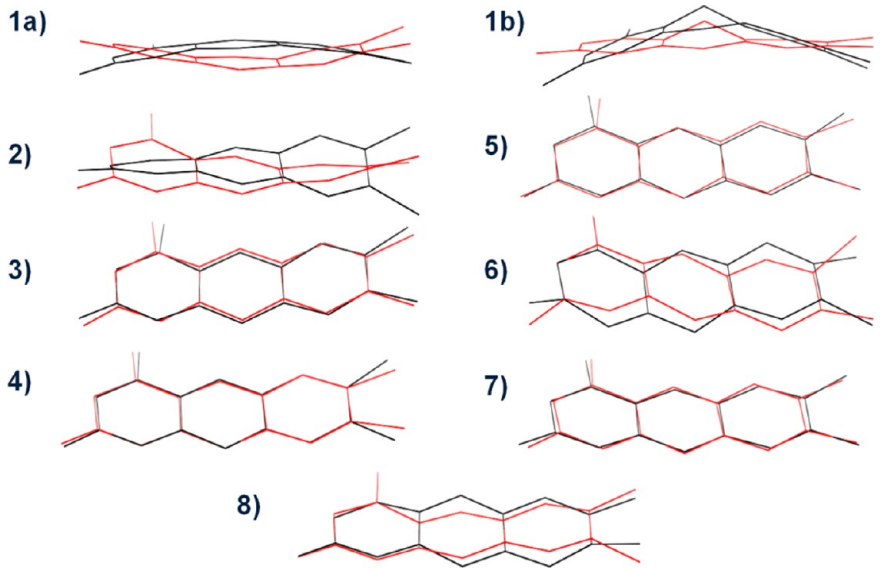

Figure 10. The superimposition of two extreme structures generated after projecting the trajectory of FOX on the first eight eigenvectors (structures from 1−8). 1a and 1b show the different collective motion of the first eigenvector in the oxidized and reduced states, respectively.

determined by NMR.[45] The inner FMN binding loop (Lβ3) contributed to the prominent collective mode of the FMN domain in the oxidized state. The outer FMN binding loop (Lβ4) contributes to the prominent collective mode of the FMN domain in the reduced state and in apoprotein. In FHQ, the major conformational change in the FMN binding site residue Trp574 was observed. Trp574 is critical to FMN cofactor binding and electron transfer in P450BM-3. In FHQ, the latter do not remain coplanar to the isoalloxazine ring to avoid the steric hindrance induced by the conformation change in the FMN cofactor upon protonation, as also suggested by ^{15}N NMR[40] and surface enhanced resonance Raman scattering[43] experiments. Hence, the change in the conformation of Trp574 might be the major factor that makes the reduced state kinetically unfavorable in P450BM-3 for transferring the electron from FMN to HEME as observed in previous studies.[46]

The FMN cofactor during simulations acquires different conformations that are mainly influenced by the movement of the ribityl side chain. The binding region of the ribityl side chain was evolutionarily more conserved. In general, the oxidized state was observed to be more flexible to obtain different conformations in the protein environment. The latter might be the result of change in the FMN binding site properties and hydrogen bond environment in the reduced state. The isoalloxazine ring of the FMN cofactor exhibits mainly eight collective motions. Except for the first vibrational modes, all modes were identical in both redox states. The FMN cofactor in the reduced state constitutes the so-called "butterfly motion" as the first collective motion due to bending of the isoalloxazine along the N5−N10 axis.

In summary, we have analyzed for the first time the dynamics of the FMN binding domain of P450BM-3 in water. In particular, we have studied the effect of FMN binding on the fluctuation modes of the FMN domain. The FMN cofactor is involved in the electron transfer in P450BM-3, and its dynamics can play an important role in electron transfer. The results of our study indicate a difference in the fluctuation amplitude of the FMN cofactor in the different redox states. The latter effect resulted from the change in the conformation of the FMN binding site due to the protonation state of the isoalloxazine ring.

■ ASSOCIATED CONTENT

Ⓢ Supporting Information

The force field parameters for the FMN cofactor in oxidized and reduced states for the GROMOS96 43a1 force field,[19] the secondary structure elements of the FMN domain, the hydrogen bond existence between FMN binding residues and the FMN cofactor, the properties (volume, hydrophobicity, solvent accessibility, and polarity) of the FMN binding pocket, RMSF and RMSD of the heavy atoms of the FMN cofactor and the cumulative sum of the number of clusters of the FMN cofactor during the simulations, the multiple sequence alignment of the FMN domain and its homologous structures, and the evolutionary conservation profile of the FMN domain are reported. This information is available free of charge via the Internet at http://pubs.acs.org

■ AUTHOR INFORMATION

Corresponding Author

*E-mail: d.roccatano@jacobs-university.de. Telephone: +49 421 200-3144. Fax: +49 421 200-3249.

Notes

The authors declare no competing financial interest.

■ ACKNOWLEDGMENTS

We thank the European Union seventh framework program (project "OXYGREEN," Project Reference: 212281) for financial support. This study was performed using the computational resources of Computer Laboratories for Animation, Modeling and Visualization (CLAMV) at Jacobs University Bremen.

■ REFERENCES

(1) Chefson, A.; Auclair, K. *Mol. Biosyst.* **2006**, *2*, 462.
(2) Wong, L. L. *Curr. Opin. Chem. Biol.* **1998**, *2*, 263.
(3) Guengerich, F. P. *Chem. Res. Toxicol.* **2001**, *14*, 611.
(4) Kumar, S. *Expert Opin. Drug Metab. Toxicol.* **2010**, *6*, 115.

(5) Warman, A. J.; Roitel, O.; Neeli, R.; Girvan, H. M.; Seward, H. E.; Murray, S. A.; McLean, K. J.; Joyce, M. G.; Toogood, H.; Holt, R. A.; Leys, D.; Scrutton, N. S.; Munro, A. W. *Biochem. Soc. Trans.* **2005**, *33*, 747.
(6) Munro, A. W.; Leys, D. G.; McLean, K. J.; Marshall, K. R.; Ost, T. W.; Daff, S.; Miles, C. S.; Chapman, S. K.; Lysek, D. A.; Moser, C. C.; Page, C. C.; Dutton, P. L. *Trends Biochem. Sci.* **2002**, *27*, 250.
(7) Girvan, H. M.; Waltham, T. N.; Neeli, R.; Collins, H. F.; McLean, K. J.; Scrutton, N. S.; Leys, D.; Munro, A. W. *Biochem. Soc. Trans.* **2006**, *34*, 1173.
(8) Jung, S. T.; Lauchli, R.; Arnold, F. H. *Curr. Opin. Biotechnol.* **2011**, *22*, 809.
(9) Whitehouse, C. J. C.; Bell, S. G.; Wong, L.-L. *Chem. Soc. Rev.* **2012**, *41*, 1218.
(10) Sevrioukova, I.; Peterson, J. A. *Biochimie* **1996**, *78*, 744.
(11) Sevrioukova, I.; Shaffer, C.; Ballou, D. P.; Peterson, J. A. *Biochemistry* **1996**, *35*, 7058.
(12) Sevrioukova, I.; Truan, G.; Peterson, J. A. *Biochemistry* **1996**, *35*, 7528.
(13) Hazzard, J. T.; Govindaraj, S.; Poulos, T. L.; Tollin, G. *J. Biol. Chem.* **1997**, *272*, 7922.
(14) Narhi, L. O.; Fulco, A. J. *J. Biol. Chem.* **1987**, *262*, 6683.
(15) Pylypenko, O.; Schlichting, I. *Annu. Rev. Biochem.* **2004**, *73*, 991.
(16) Chen, H. C.; Swenson, R. P. *Biochemistry* **2008**, *47*, 13788.
(17) Sevrioukova, I. F.; Hazzard, J. T.; Tollin, G.; Poulos, T. L. *J. Biol. Chem.* **1999**, *274*, 36097.
(18) Sevrioukova, I. F.; Li, H. Y.; Zhang, H.; Peterson, J. A.; Poulos, T. L. *Proc. Natl. Acad. Sci. U. S. A.* **1999**, *96*, 1863.
(19) van Gunsteren, W. F.; Billeter, S. R.; Eising, A. A.; Hunenberger, P. H.; Kruger, P.; Mark, A. E.; Scott, W. R. P.; Tironi, I. G. *GROMOS96*; VdF Hochschulverlag AG an der ETH Zurich: Zurich; BIOMOS b.v.: Groningen, 1996.
(20) Abe, M.; Kyogoku, Y. *Spectrochim. Acta, Part A* **1987**, *43*, 1027.
(21) *ACD/ChemSketch Freeware*, version 12.01; Advanced Chemistry Development, Inc.: Toronto, ON, Canada, 2010.
(22) Berendsen, H. J. C.; Postma, J. P. M.; van Gunsteren, W. F.; Hermans, J. *Intermol. Forces* **1981**, 331.
(23) Zheng, Y.-J.; Ornstein, R. L. *J. Am. Chem. Soc.* **1996**, *118*, 9402.
(24) Walsh, J. D.; Miller, A. F. *J. Mol. Struct.: THEOCHEM* **2003**, *623*, 185.
(25) Hess, B.; Bekker, H.; Berendsen, H. J. C.; Fraaije, J. G. E. M. *J. Comput. Chem.* **1997**, *18*, 1463.
(26) Miyamoto, S.; Kollman, P. A. *J. Comput. Chem.* **1992**, *13*, 952.
(27) Darden, T.; York, D.; Pedersen, L. *J. Chem. Phys.* **1993**, *98*, 10089.
(28) Berendsen, H. J. C.; Postma, J. P. M.; Vangunsteren, W. F.; Dinola, A.; Haak, J. R. *J. Chem. Phys.* **1984**, *81*, 3684.
(29) Hess, B.; Kutzner, C.; van der Spoel, D.; Lindahl, E. *J. Chem. Theory Comput.* **2008**, *4*, 435.
(30) Daura, X.; Gademann, K.; Jaun, B.; Seebach, D.; van Gunsteren, W. F.; Mark, A. E. *Angew. Chem., Int. Ed.* **1999**, *38*, 236.
(31) Schmidtke, P.; Bidon-Chanal, A.; Luque, F. J.; Barril, X. *Bioinformatics* **2011**, *27*, 3276.
(32) *The PyMOL Molecular Graphics System*, version 1.5.0.4; Schrödinger, LLC: New York, 2012.
(33) Altschul, S. F.; Gish, W.; Miller, W.; Myers, E. W.; Lipman, D. J. *J. Mol. Biol.* **1990**, *215*, 403.
(34) Bernstein, F. C.; Koetzle, T. F.; Williams, G. J.; Meyer, E. F., Jr.; Brice, M. D.; Rodgers, J. R.; Kennard, O.; Shimanouchi, T.; Tasumi, M. *J. Mol. Biol.* **1977**, *112*, 535.
(35) Pettersen, E. F.; Goddard, T. D.; Huang, C. C.; Couch, G. S.; Greenblatt, D. M.; Meng, E. C.; Ferrin, T. E. *J. Comput. Chem.* **2004**, *25*, 1605.
(36) Amadei, A.; Linssen, A. B.; Berendsen, H. J. *Proteins* **1993**, *17*, 412.
(37) Amadei, A.; Linssen, A. B.; de Groot, B. L.; van Aalten, D. M.; Berendsen, H. J. *J. Biomol. Struct. Dyn.* **1996**, *13*, 615.
(38) Amadei, A.; Ceruso, M. A.; Di Nola, A. *Proteins* **1999**, *36*, 419.
(39) Kabsch, W.; Sander, C. *Biopolymers* **1983**, *22*, 2577.
(40) Kasim, M.; Chen, H. C.; Swenson, R. P. *Biochemistry* **2009**, *48*, 5131.
(41) Haines, D. C.; Sevrioukova, I. F.; Peterson, J. A. *Biochemistry* **2000**, *39*, 9419.
(42) Nakai, S.; Yoneda, F.; Yamabe, T. *Theor. Chem. Acc.* **1999**, *103*, 109.
(43) Macdonald, I. D. G.; Smith, W. E.; Munro, A. W. *Eur. Biophys. J.* **1999**, *28*, 437.
(44) Wittung-Stafshede, P. *Acc. Chem. Res.* **2002**, *35*, 201.
(45) Sibille, N.; Blackledge, M.; Brutscher, B.; Coves, J.; Bersch, B. *Biochemistry* **2005**, *44*, 9086.
(46) Klein, M. L.; Fulco, A. J. *J. Biol. Chem.* **1993**, *268*, 7553.